Industrial Crops & Products 202 (2023) 117044

Contents lists available at ScienceDirect

Industrial Crops & Products

journal homepage: www.elsevier.com/locate/indcrop

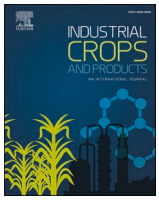

Integrating genetic-engineered cellulose nanofibrils of rice straw with mild chemical treatments for enhanced bioethanol conversion and bioaerogels production

Zhen Hu [a,b,1], Hao Peng [a,b,1], Jingyuan Liu [b], Huiyi Zhang [b], Sufang Li [b], Hailang Wang [b], Zhengyi Lv [b], Youmei Wang [b], Dan Sun [c], Jingfeng Tang [a], Liangcai Peng [a,b], Yanting Wang [a,b,*]

[a] Key Laboratory of Fermentation Engineering (Ministry of Education), National "111" Center for Cellular Regulation & Molecular Pharmaceutics, Cooperative Innovation Center of Industrial Fermentation (Ministry of Education & Hubei Province), Hubei Key Laboratory of Industrial Microbiology, College of Biotechnology & Food Science, Hubei University of Technology, Wuhan 430068, China
[b] Biomass & Bioenergy Research Center, College of Plant Science & Technology, Huazhong Agricultural University, Wuhan 430070, China
[c] School of Material Science & Chemical Engineering, Hubei University of Technology, Wuhan 430068, China

ARTICLE INFO

Keywords:
Cellulose
Bioethanol
Bioaerogels
OsCESA7
Site-mutation
Rice straw

ABSTRACT

Cellulose in crop straws represents an abundant biopolymer convertible for biofuels and bioproducts, while the inherent recalcitrance of lignocellulose limits these applications. By selecting desirable rice mutant (*cesa7*) from site-mutation of the OsCESA7 isoform essential for cellulose biosynthesis, this study examined much improved lignocellulose recalcitrance such as reduced cellulose crystallinity, polymerization and nanofibril length for increased lignocellulose porosity and accessibility. Compared with its wild type, the *cesa7* mutant showed a near-complete biomass saccharification with hexose yields of over 96% (% cellulose) for bioethanol production raised by 58%– 71% under three green-like pretreatments performed. Meanwhile, the cellulose substrate of *cesa7* mutant was applied to produce aerogels with high porosity and large specific surface under less-intensity ultrasonic treatment, and its further mild chemical modification led to significantly raised oil adsorption capacity by 55%, mainly due to higher proportion of nanofibrils and the honeycomb-like fibers structure observed. It has thus provided an applicable approach for high-yield bioethanol and high-quality aerogels by integrating genetic-modified cellulose substrates with cost-effective process technology.

1. Introduction

As carbon neutralization is a long-term goal for globe warming climate control, the development of a low carbon bioeconomy has been considered as a promising solution (Xu et al., 2022). In particular, the green biorefinery of crop lignocellulose residues is increasingly conducted for sustainable energy and degradable biomaterials (Teo and Wahab, 2020; Wang et al., 2021). As the most renewable biopolymer on the earth, lignocellulose has been implemented for the development of environmentally friendly biofuels and highly valuable bioproducts including cellulosic ethanol and cellulose aerogels (Dilamian and Noroozi, 2021; Hu et al., 2023). However, because lignocellulose is of extremely recalcitrant property against its enzymatic degradation and chemical conversion, current biomass process technology principally requires harsh reaction conditions with potential secondary pollution (Bhatia et al., 2020).

Cellulose is composed of the β-1, 4-glucan chains that assemble into cellulose microfibrils primarily via hydrogen bonds. The crystalline cellulose microfibrils provide mechanical strength to plant tissues and also exhibit major recalcitrance against biomass enzymatic hydrolysis (Himmel et al., 2007; Liu et al., 2016). Particularly, both the degree of polymerization (DP) and crystallinity index (CrI) of cellulose have been identified as two major parameters accounting for lignocellulose recalcitrance in plants (Deng et al., 2020; Fu et al., 2022; Sun et al., 2020). To

* Corresponding author at: Key Laboratory of Fermentation Engineering (Ministry of Education), National "111" Center for Cellular Regulation & Molecular Pharmaceutics, Cooperative Innovation Center of Industrial Fermentation (Ministry of Education & Hubei Province), Hubei Key Laboratory of Industrial Microbiology, College of Biotechnology & Food Science, Hubei University of Technology, Wuhan 430068, China.
E-mail address: wyt@mail.hzau.edu.cn (Y. Wang).
[1] Equal contribution

https://doi.org/10.1016/j.indcrop.2023.117044
Received 7 February 2023; Received in revised form 7 May 2023; Accepted 13 June 2023

reduce lignocellulose recalcitrance, genetic modification of plant cell walls has been conducted by creating the genetic mutants and transgenic lines that are silent or overexpressing the genes involved in cellulose biosynthesis and modification in bioenergy crops (Fan et al., 2017; Huang et al., 2019; Li et al., 2018). As cellulose is the major component of plant cell walls, appropriately minor modification of cellulose microfibrils is crucial to maintain plant lodging resistance and growth and also to enhance lignocellulose enzymatic hydrolysis and chemical conversion under relatively mild process conditions (Zhang et al., 2023).

Cellulosic ethanol has been regarded as a remarkable additive into petroleum fuels with lower net carbon release. Principally, cellulosic ethanol production includes three major processes: initial biomass pretreatment, subsequent saccharification, and final ethanol fermentation (Hu et al., 2021). Particularly, despite chemical and physical pretreatments are broadly applied to improve enzymatic saccharification in diverse lignocellulose residues, the high capital costs of harsh pretreatments and the difficulties to recycle of chemicals result in a negative environmental impact (Cantero et al., 2019). Therefore, attempts have been recently made by combining green-like pretreatments with recalcitrance-reduced lignocellulose residues for cost-effective bioethanol conversion (Li et al., 2018; Wu et al., 2019). For instances, CaO and green liquid pretreatments have been performed for chemical recyclable (Alam et al., 2020; Gao et al., 2021), whereas liquid hot water (LHW) is applied as non-chemical pretreatment (Wu et al., 2019).

Cellulose microfibrils are applicable to generate aerogels for efficient separation of non-polar hydrocarbon and petrol oil (Dilamian and Noroozi, 2021; Thai et al., 2020). Since cellulose aerogels are of relatively higher adsorption capacity and biodegradability compared to other chemically-synthetized sorbents, attention has been paid to improve cellulose aerogels properties and also to reduce its expense (Chen et al., 2021; Jiang and Hsieh, 2017; Zhang et al., 2019). Despite it has been characterized that the traditional cellulose aerogel process requires fibrillation, gelling and drying (Jiang et al., 2013), much is unknown about the desirable cellulose substrates that are favor for aerogel production at high quality with relatively low cost.

Rice represents a staple food crop around the world and produces abundant lignocellulose-rich straw for the development of cellulosic ethanol and cellulose aerogel (Bhattacharyya et al., 2019; Dilamian and Noroozi, 2021; Li et al., 2018). In this study, a CRISPR/Cas9 technology was applied to generate specific site-mutant (*cesa7*) of the OsCESA7 that is essential for cellulose biosynthesis in rice (Tanaka et al., 2003). We then observed normal growth phenotypes and enhanced lodging resistance in the *cesa7* mutant. Furthermore, we determined significantly reduced cellulose DP, CrI and nanofibril length in the *cesa7* mutant for much raised lignocellulose accessibility and porosity, leading to a near-complete biomass enzymatic saccharification achieved for high bioethanol production under three green-like pretreatments performed. Notably, this study generated high quality of cellulose aerogels from the *cesa7* mutant straw compared to its wild type under mild ultrasound conditions. Therefore, this study provided a powerful strategy for high cellulose ethanol and aerogel production by integrating genetic modification of cellulose microfibrils with mild biomass process technology.

2. Materials and methods

2.1. Creation of rice cesa7 mutant

The rice *cesa7* mutant was created via a previously established CRISPR/Cas9 method (Xie et al., 2015). The sgRNA targeting *OsCESA7* gene was designed based on the NPB reference genome using the CRISPR-PLANT web-tool (Xie et al., 2014). The sgRNA array was linked into the pRGEB32 vector and transformed into NPB calli. A *Cas9* gene specific primer was used to select the transgenic positive lines. Sanger sequencing was conducted to check genomic mutants. The CRISPR-P program was employed to identify the potential off-target sites (Liu et al., 2017), which were subsequently checked by Sanger sequencing. The specific primers used for selecting transgenic positive lines and detecting on-target or off-target mutations were listed in Table S1. The experimental process for creation of the *cesa7* mutant was shown in Fig. S1.

2.2. Evaluation of agronomic traits and mechanical character

Lodging index (*LI*) of rice plant at 30 days after flowering was detected as previously described by Hu et al. (2018). Firstly, the breaking force (*BF*) of second internode was measured using a plant lodging tester (DIK 7400, Japan). Then the length (*L*) and the weight (*W*) of the section from the breaking site to the panicle were measured by meter ruler and electronic scales. The *LI* of rice plant was calculated via the Eq. (1):

$$LI = \frac{L \times W \times 9.8}{BF \times 5 \times 1000} \times 100 \quad (1)$$

The extension force of rice stem was tested as previously described (Zhang et al., 2016). The second internodes at rice milk maturity stage were cut to 10 cm in length, and their stretching force before being broken was recorded by a force tester (RH-K300, China). The plant height, seed yields and biomass yields were measured after harvest. All traits were measured under ten independent biological duplicates.

2.3. Determination of plant cell wall structure and composition

Safranin staining and observation of sclerenchyma cells in rice second internodes at heading stage was performed as described by Ma et al. (1993). Transmission electron microscopy observation of sclerenchyma cells in the leaf veins of one-month old rice plants was conducted as described by Peng et al. (2022). Cell wall polysaccharides were measured by continuous extraction method as described by Fu et al. (2022). Hemicellulose monosaccharides were measured by GC-MS method as described by Xu et al. (2012). Total lignin was determined by two-step acid hydrolysis method (Huang et al., 2017). Monolignols of lignin samples were extracted by nitrobenzene oxidation method and measured by HPLC analysis (Zhang et al., 2020).

2.4. Detection of cellulose features

Cellulose CrI was determined by the X-ray diffraction method as described by Li et al. (2018). Rice biomass powders were placed in the glass holder and scanned under plateau conditions. The radiation was generated at 40 kV and 18 mA, and scanned at a rate of 0.0197°/s from 10° to 45°. The CrI value was calculated according to the intensity of the 200 peak (I_{200}, $2\theta = 22.5°$) and the 110 peaks (I_{am}, $2\theta = 18.5°$) via the Eq. (2).

$$\mathrm{CrI}(\%) = \frac{I_{200} - I_{am}}{I_{200}} \times 100 \quad (2)$$

The cellulose DP were determined by the viscometry method (Deng et al., 2020), and calculated according to the Eq. (3), where $[\eta]$ represents the intrinsic viscosity of the solution that was determined by interpolation using the USP table that illustrated predetermined values of the product of concentration and intrinsic viscosity.

$$\mathrm{DP}^{0.905} = 0.75 \times [\eta] \quad (3)$$

Congo Red stain was conducted as previously described by Alam et al. (2019). About 50 mg crude cellulose was incubated with Congo Red solution in 0.3 M phosphate buffer at 60 °C for 24 h. The concentrations of Congo Red were set as 0.25, 0.5, 1.0, 1.5, 2.0, 4.0, 5.0, 6.0, 7.0, 8.0 g/L, respectively. After centrifugation at 8000 *g* for 5 min, the supernatant was collected and the absorbance was measured at 498 nm. The monolayer *Langmuir* adsorption model was used to calculate the adsorption capacity of cellulose samples.

The amount of reducing ends of cellulose was assayed using the CBHI

enzyme hydrolysis method as previously described (Huang et al., 2019) with minor modification. The crude cellulose samples (0.05 g) were incubated with 0.3 U CBHI (E.C. 3.2.1.91, Megazyme, USA) at 50 °C for 1.5, 3, 6, 12 and 24 h, respectively. After centrifugation at 8000 *g* for 5 min, the released hexoses yield of supernatant was determined by GC-MS method.

In situ AFM observation of cellulose microfibrils in rice cell wall was conducted as described by Peng et al. (2022). The sections of rice second internodes were incubated with 8% acidic chlorite (including 1 mM HCl) at 50 °C for 48 h. After washed with dH_2O for six times, the sections were observed by using an AFM machine (CSPM5500).

2.5. Biomass pretreatment, enzymatic hydrolysis and yeast fermentation

The CaO pretreatment and LHW pretreatment were conducted as previously described by Jin et al. (2016), and the green liquor (GL, mixed Na_2S and Na_2CO_3) pretreatment were conducted as described by Alam et al. (2020). For CaO pretreatment, biomass powder (0.30 g) was treated with 6 mL 5% CaO (w/w) for 2 h at 50 °C. For LHW pretreatment, the biomass powder was added with 3 mL H_2O into stainless steel bombs, and heated at 200 °C with 15 rpm shaken for 0.5 h. For GL pretreatment, the biomass powder was treated with 3 mL GL solution (30% sulfidity) and impregnated at 60 °C for 0.5 h. Then the temperature was raised to 150 °C and maintained for 20 min. After pretreatment, the residues were washed by H_2O and acetate buffer (pH 4.8), and then incubated with mixed-cellulases, while 1% Tween-80 (v/v) was co-supplied. Biomass enzymatic hydrolysis was performed at 50 °C under 150 rpm shaken at a time course of reactions. Yeast fermentation was performed as previously described by Li et al. (2017). After activation, yeast (Angel yeast Co., Ltd., China) was inoculated into the mixture of enzymatic hydrolysates and residues. The fermentation was performed at 37 °C for 48 h. Ethanol content was measured by the $K_2Cr_2O_7$ method (Fletcher and van Staden, 2003). The experiment for biomass process was shown in Fig. S1.

2.6. Preparation and stability analysis of cellulose suspension

The purification and fibrillation of cellulose fibers was performed as previously described (Dilamian and Noroozi, 2021) with minor modification. The biomass powder samples (20 g) were incubated with 600 mL 5% NaOH at 60 °C for 2 h with 5 times, and then incubated with 600 mL 8% $NaClO_2$ (pH 4.5) at 25 °C for 6 h with 3 times. The solid residues were filtered and washed with H_2O to neutral. The purified cellulose was treated with an ultrasonic processor (JY92-IIDN, China) at 22 kHz with an output power of 600 W for 2.5–20 min to achieve cellulose suspension. The ultrasonic process was carried out at the temperature below 4 °C. For the stability analysis, the cellulose suspensions were injected into water by a 1000 μL pipette gun, and the morphology was photographed. Centrifugal sedimentation was conducted from 1000 *g* to 12000 *g*, and the height of final cellulose suspensions and initial aqueous suspensions were recorded. What's more, 0.8% (m/v) cellulose suspensions were diluted into 0.04%– 0.4%, and the final height of cellulose suspensions at various dilute concentrations was recorded after set aside for 12 h.

2.7. Fabrication and modification of cellulose aerogels

The fabrication and modification of cellulose aerogels were conducted as previously described (Wang et al., 2015). The 10 mL cellulose suspensions at various dilute concentrations (0.04%−0.4%, m/v) were transferred to a plastic cup and frozen at − 22 °C for 12 h. The samples were then lyophilized in a vacuum freeze-drier (FD-1A-50, China) at − 55 °C and a pressure of 15 bar for 60 h to fabricate cellulose aerogels. A chemical vapor deposition process was conducted for hydrophobic coating of methyltrimethoxysilane (MTMS). In detail, two small plastic sample cups containing 3 mL MTMS and 3 mL deionized water were placed in a 1 L glass bottle of cellulose aerogels. The glass bottle was tightly sealed and placed at 70 °C for 3 h. Finally, the silanized samples were placed in a vacuum oven for 24 h at 60 °C to remove the unreacted silane. The experiment for fabrication and modification of cellulose aerogels was shown in Fig. S1.

2.8. Assessment of cellulose aerogels properties

The apparent weight and volume of cellulose aerogels were respectively measured using an analytical balance and a digital caliper with 0.1 mg and 0.01 mm resolution. The shape of aerogels was regarded as a cylinder. The porosity of aerogels was measured according to the Eq. (4), where ρ_a is the density of aerogel and ρ_b is the density of crystalline cellulose (1.5 g/cm^3) (Zheng et al., 2014).

$$\text{Porosity}(\%) = \left(1 - \frac{\rho_a}{\rho_b}\right) \times 100 \quad (4)$$

The BET specific surface area of cellulose aerogels was determined by N_2 physisorption at 77 K using a surface area analyzer (Micrometrics ASAP 2460, USA). The structure of dispersed cellulose fibers and fabricated aerogels were observed using a scanning electron microscopy (Hitachi SU8020). FTIR spectroscopy was scaned using a PerkinElmer spectrophotometer (Nicolet Nexus 470, USA). Water contact angle were measured on a contact angle tester (OCA20, German) using a droplet (3 μL) of deionized water as an indicator at 25 °C. The compressive properties of the cellulose aerogels were determined using a computerized electronic universal testing machine (UTM2103, Suns Technology Stock Co., Ltd, China) equipped with a 100 N load cell. A deformation rate of 3 mm/min was applied on the top surface of each sample until the deformation of the sample exceeded 80%.

2.9. Measurement of oil adsorption capability

The maximum oil adsorption capability of MTMS modified cellulose aerogels was measured as previously described (Thai et al., 2020). The modified cellulose aerogels were weighed before immersing into 200 mL vacuum pump oil (Great Wall No.1, China; $\rho = 0.88$ g/cm^3) for 10 min. The aerogels were weighted again after draining off the excess oil for 1 min. The oil adsorption capacity of aerogels was determined according to the Eq. (5), where Q (g/g) represents the oil absorption capacity; m_1 (g) and m_2 (g) represent the aerogel weights before and after oil absorption, respectively.

$$Q = \frac{m_2 - m_1}{m_1} \quad (5)$$

The circulating oil absorption performance of cellulose aerogels was tested using a repeated adsorption-desorption method. After adsorption, the aerogel was washed four times with 100 mL hexane and then dried in a vacuum oven at 65 °C for 3 h before the next cycle of adsorption. This process was repeated five times and the amount of oil absorbed was recorded after each cycle.

3. Results and discussion

3.1. Selection of rice mutant (cesa7) from site-specific mutation of OsCESA7 for cellulose biosynthesis

By means of CRISPR/Cas9 gene editing system, this study generated a novel rice mutant (*cesa7*) by site-specific mutation of the *OsCESA7* gene (Fig. 1), which has been examined as one isoform of cellulose synthase complexes essential for cellulose biosynthesis of secondary cell walls in rice (Tanaka et al., 2003). The rice *cesa7* mutant exhibited a single amino acid (E_{417}) deletion in the plant-conserved region (P-CR) of OsCESA7 protein, and seven of the most potential off-target sites in the *cesa7* mutant were checked by Sanger sequencing, indicating no occurrence of the off-target mutations (Fig. 1 A-C; Table S2). To evaluate

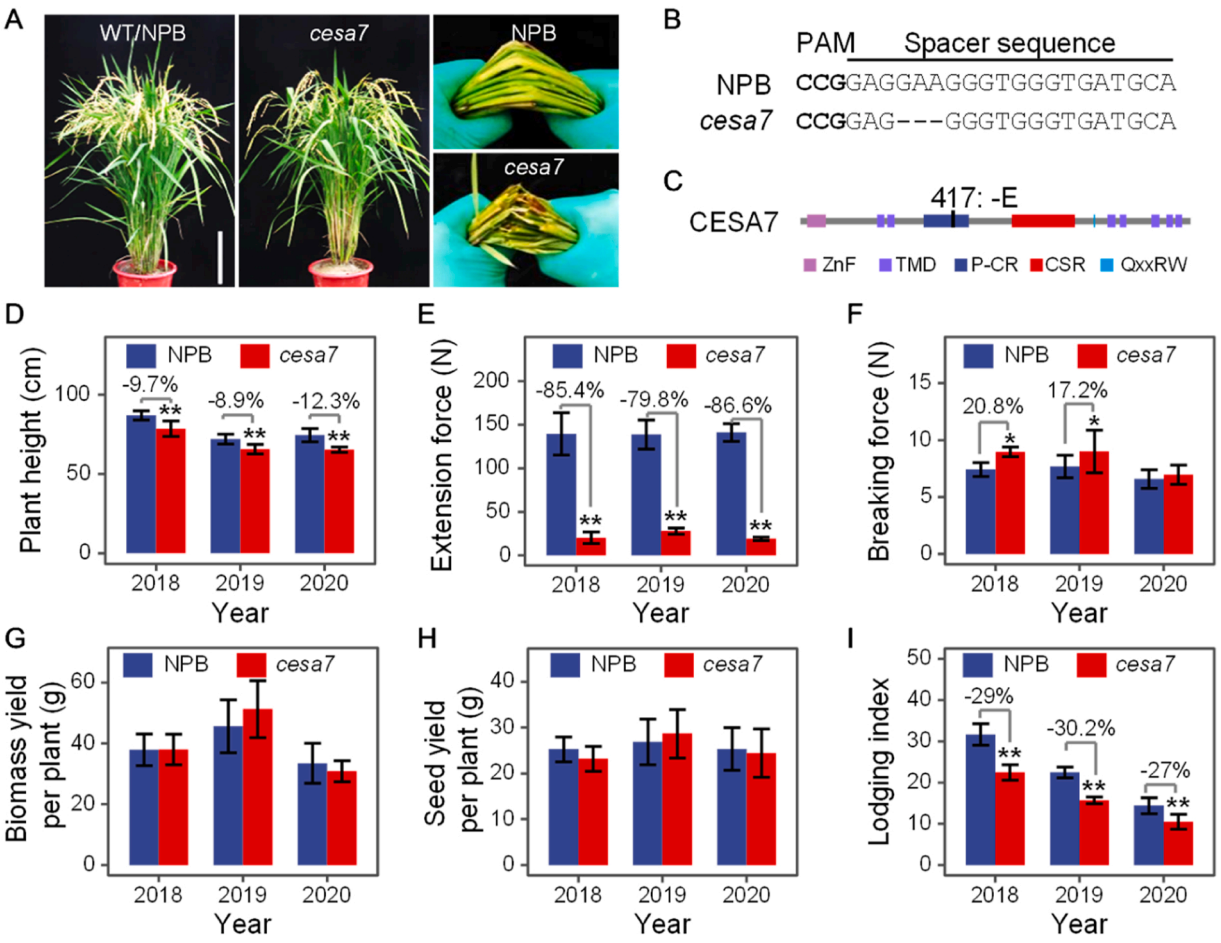

Fig. 1. Selection of rice mutant (*cesa7*) from site mutation of OsCESA7. (A) Mature plants of wild type (NPB) and *cesa7* mutant at 30 days after flowering with manual-bended culms phenotypes, Bar = 20 cm. (B) CRISPR/Cas9-induced 3 bp deletion in *OsCESA7* gene of *cesa7* mutant. (C) An amino acid (E_{417}) deletion in the P-CR region of OsCESA7 protein of *cesa7* mutant. (D-I) Plant height (D), extension force (E), breaking force (F), biomass yield (G), seed yield (H) and lodging index (I) of NPB and *cesa7* mutant plant from 3-year field experiments. Increased or decreased percentage was obtained by subtraction between the data of *cesa7* mutant and NPB divided by the NPB (n = 10). * and * * indicated significant difference between two samples by *t*-test at $p < 0.05$ and 0.01, respectively.

OsCESA7 site-mutation impact on plant growth and development, this study detected plant height, stem mechanical strength, lodging resistance and seed and biomass yields in the *cesa7* mutant from consistent three-year field experiments (Fig. 1 D-I). As a result, the *cesa7* mutant was of typically culm-brittle phenotype with the extension force reduced by 79.8%− 86.6%, while its breaking force was not decreased compared to its wild type (NPB) (Fig. 1 E, F). Despite the *cesa7* mutant exhibited relatively shorter plant height by 10%, its seed and biomass yields were not significantly altered (Fig. 1 G, H). Notably, this study examined consistently reduced lodging index values in the *cesa7* mutant by 27%− 30.2% from three-year field experiments accounting for significantly raised plant lodging resistance (Fig. 1 I), which was consistent with the nature mutant (*Osfc16*) as previously reported (Li et al., 2017).

3.2. Altered cell wall structure and cellulose features in the cesa7 mutant

Using typical safranin staining with stem tissues at the seedling stage of rice, we observed less intensity of pink color accountable for thinner cell walls in the vascular bundle tissue of *cesa7* mutant, compared to the NPB (Fig. 2 A). Under transmission electron microscopy, the *cesa7* mutant exhibited significantly lessened secondary cell walls and entire cell walls at $p < 0.01$ levels (Fig. 2 B, C). Chemical analysis further indicated that the cellulose content was decreased by 23.7% in mature rice straw in the *cesa7* mutant, but hemicellulose and lignin levels were raised by 14.8% and 9.4% with similar pectin level to the NPB (Fig. 2 D). The raised hemicellulose and lignin should compensate for reduced cellulose in the *cesa7* mutant, resulting in similar biomass yield examined. Furthermore, this study detected multiple cellulose features including cellulose CrI and DP values, the amount of reducing end of β-1, 4-glucan chains, cellulose accessibility and nanofibril length (Fig. 3). Compared to the NPB, the *cesa7* mutant showed either lower CrI by 11.8% or less DP values by 14.8% and 30.5% in two types of celluloses substrates (Fig. 3 A, B). Using the cellobiohydrolase (CBHI) specific for enzymatic hydrolysis starting from reducing ends of β-1, 4-glucan chains, we examined much higher glucose yields released from the time-course enzymatic hydrolyses of the *cesa7* mutant than those of the NPB (Fig. 3 C), consistent with its significantly reduced cellulose DP value and relatively raised reducing ends of β-1, 4-glucan chains. As the Congo red staining is applicable to estimate cellulose surface area and the *Langmuir* isothermal adsorption model enables to obtain the maximum adsorption capacity (q_{max}) for cellulose accessibility (Alam et al., 2019), this study evaluated the q_{max} value increased by 10.6% accountable for larger surface area of cellulose microfibrils in the *cesa7* mutant, compared to the NPB (Fig. 3 D). Adopting our recently-developed AFM approach (Peng et al., 2022), this study detected the lengths of cellulose nanofibrils in the *cesa7* mutant was decreased 23.5% (Fig. 3 E, F), which was consistent with either much reduced cellulose CrI and DP values or raised cellulose accessibility in the mutant. Because the cellulose CrI and DP are two major causes of lignocellulose recalcitrance and the cellulose reducing-ends amount and accessibility are two positive factors on biomass enzymatic saccharification (Sun et al., 2020; Xu et al., 2012), the results demonstrated that

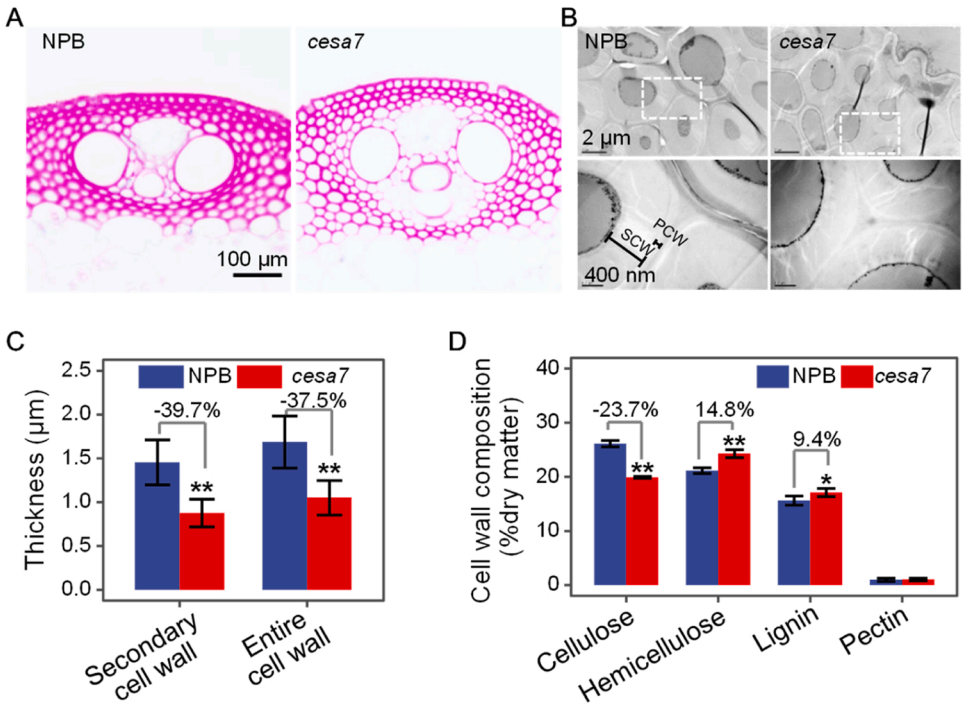

Fig. 2. Plant cell wall structures and compositions of NPB and *cesa7* mutant plant. (A) Sclerenchyma cells with safranin staining under an optical microscope, scale bar as 100 μm. (B) Cell walls of sclerenchyma tissues under transmission electron microscopy, PCW as primary cell wall, SCW as secondary cell wall, scale bar as 2 μm (up) and 400 nm (down). (C) Quantitative measurement of cell wall thickness (n = 20). (D) Cell wall composition of mature stem tissues (n = 3). Increased or decreased percentage was obtained by subtraction between the data of *cesa7* mutant and NPB divided by the NPB. * and * * indicated significant difference between two samples by *t*-test at $p < 0.05$ and 0.01, respectively.

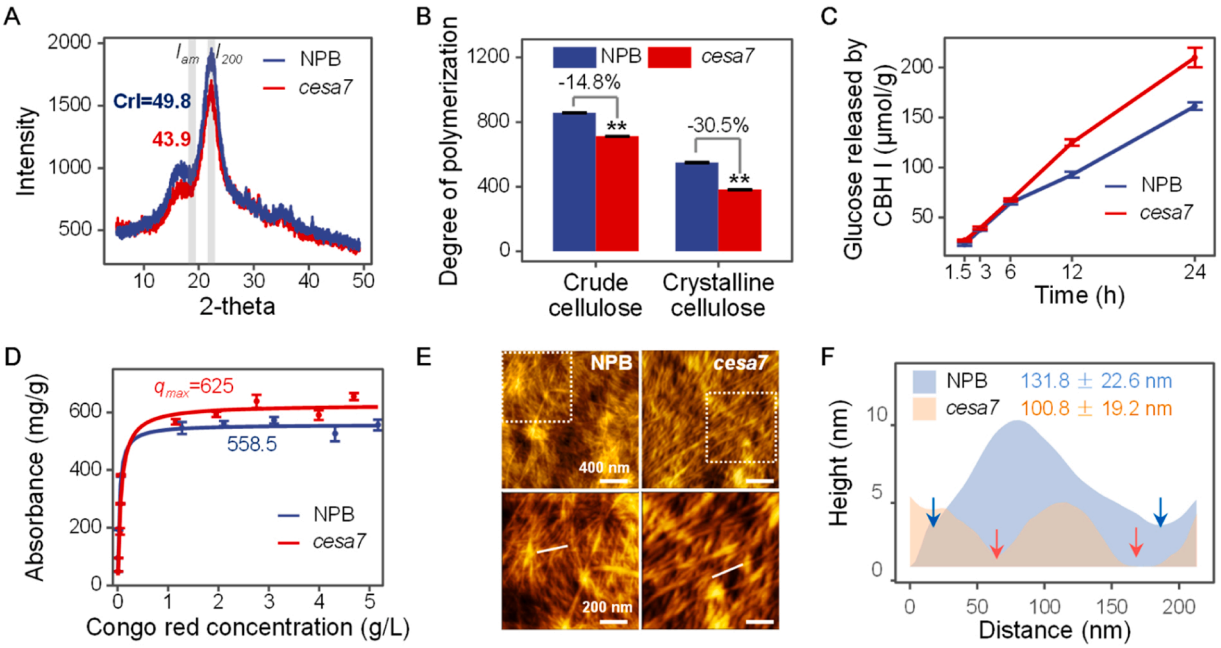

Fig. 3. Cellulose features in mature straws of NPB and *cesa7* mutant. (A) Cellulose crystalline index. (B) Degree of polymerization of crude cellulose and crystalline cellulose substrates. (C) Glucose yield released from time-course CBHI hydrolysis of the crude cellulose substrates. (D) Congo red adsorption of crude cellulose substrates, and the maximum adsorption capacities (q_{max}) obtained by data fitting using *Langmuir* isothermal adsorption model. (E) AFM images of plant cell wall treated by 8% chlorite. The upper AFM images highlighted within white boxes were magnified below as scaled at 200 nm. (F) Evaluation of the average distance between two defects on the surfaces of the cellulose nanofibrils as highlighted in (E) to present the nanofibril length. The data as mean ± SD (n = 100).

the site-mutation of OsCESA7 could modify multiple cellulose features for remarkably reduced lignocellulose recalcitrance in rice straw. In addition, the *cesa7* mutant did not show much alteration of either hemicellulose monosaccharide composition or three lignin monomer proportion (Table S3, S4), confirming that the *cesa7* mutant should be of specifically-modified cellulose substrate.

3.3. Improved biomass saccharification and bioethanol production under green-like pretreatments

Since the *cesa7* mutant was of recalcitrance-reduced lignocellulose as described above, biomass enzymatic saccharification was examined by measuring hexose yield (% cellulose) released from enzymatic hydrolysis of pretreated lignocellulose residues (Fig. 4). By performing three green-like (chemical recyclable or non-chemical) pretreatments as

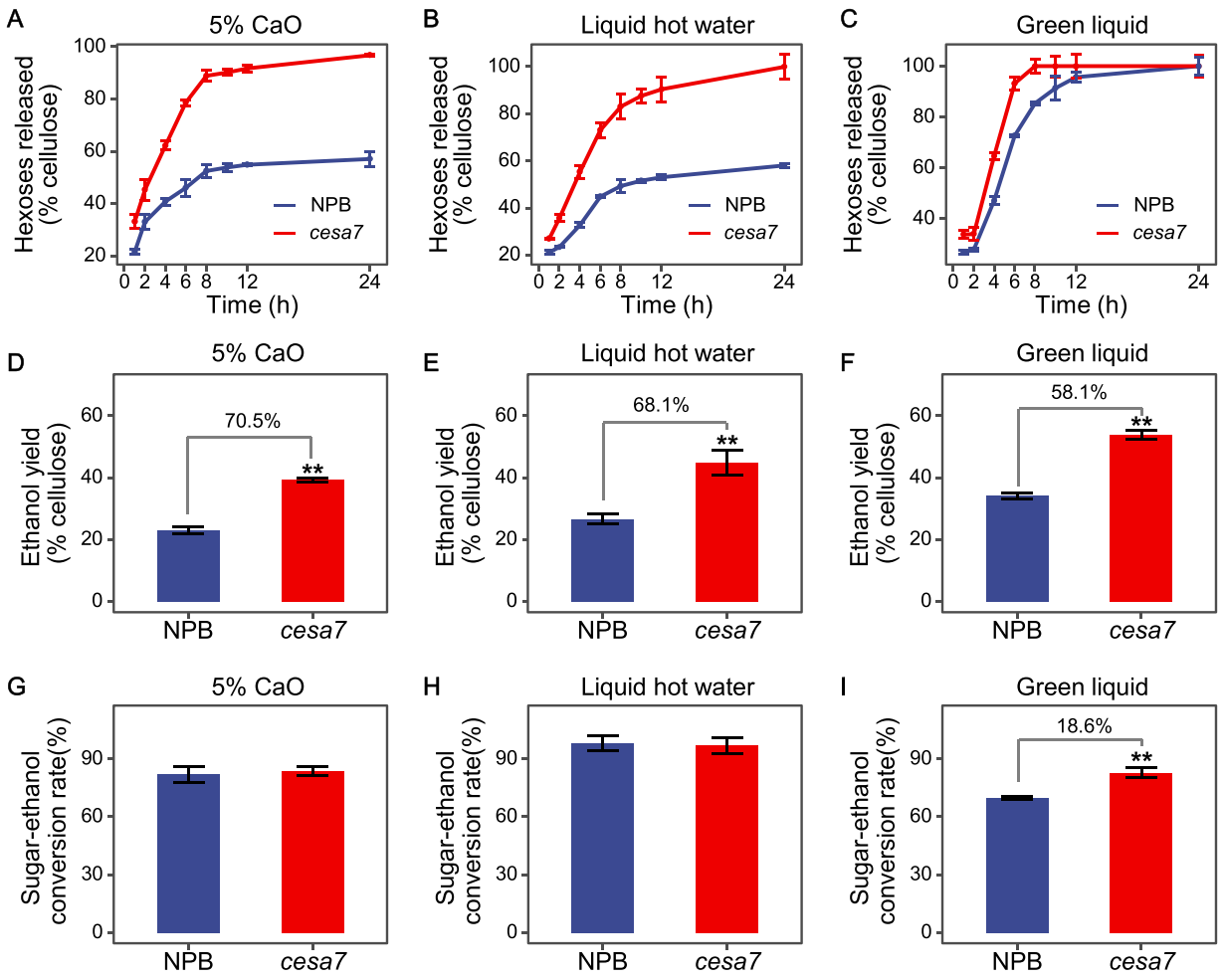

Fig. 4. Biomass enzymatic saccharification and bioethanol production of *cesa7* mutant and NPB. (A-C) Hexose yields (% cellulose) released from time-course enzymatic hydrolysis after 5% CaO pretreatment (A), liquid hot water pretreatment (B) or green liquid pretreatment (C). (D-F) Bioethanol yields obtained from yeast fermentation using total hexoses released from enzymatic hydrolysis. (G-I) Sugar-ethanol conversion rates. Increased percentage was obtained by subtraction between the data of *cesa7* mutant and NPB divided by the NPB. * and * * indicated significant difference between two samples by *t*-test at $p < 0.05$ and 0.01, respectively.

previously established (Alam et al., 2020; Wu et al., 2019), we detected remarkably enhanced hexose yields in the *cesa7* mutant, compared to the NPB (Fig. 4 A-C). Particularly, three green-like pretreatments could lead to near-complete enzymatic saccharification with hexose yields of more than 96% (% cellulose), whereas the NPB had the hexoses yields of less than 60% from the CaO and LHW pretreatments. Further comparison with other rice straw processing in previous studies, the *cesa7* mutant showed higher hexoses yields released from much less time of enzymatic hydrolysis even though under relatively mild green-like pretreatments (Table 1). Using all hexoses for yeast fermentation, this study consequently detected that the *cesa7* sample was of significantly higher bioethanol yields than those of the NPB sample, with raised ethanol rates at 58%, 68% and 71% from three pretreatments performed (Fig. 4 D-F). Despite of similar sugar-ethanol conversion rates under CaO and LHW pretreatments, the *cesa7* sample was of significantly higher conversion rate by 19% than that of the NPB at $p < 0.01$ level under the green liquid pretreatment (Fig. 4 G-I), suggesting that less toxic compounds should be produced from the green liquid pretreatment in the *cesa7* mutant. Therefore, due to multiple modifications of cellulose features, the *cesa7* sample was of consistently enhanced biomass saccharification and bioethanol production under green-like pretreatments.

Table 1
Comparison of hexose yields obtained from enzymatic hydrolysis of pretreated rice straws with previous works.

Rice plants	Pretreatment	Enzymatic hydrolysis time (h)	Hexose yield (% cellulose)	Reference
***cesa7* mutant**	**5% CaO, 50 °C for 2 h**	**24**	**96.9%**	**This study**
	Liquid hot water, 200°C for 30 min	**24**	**100.0%**	
	Green liquid (30% sulfidity), 150 °C for 20 min	**8**	**100.0%**	
Wild type	Sulfur trioxide for 4 h and 1% NaOH at 50 °C for 7 h	48	91.0%	(Yao et al., 2011)
Wild type	Green liquid (20% sulfidity), 140 °C for 1 h	48	92.5%	(Gu et al., 2013)
Wild type	Steam explosion at 170 °C for 10 min and 2% KOH at 121 °C for 30 min	48	82.6%	(Banoth et al., 2017)
Wild type	1.5% NaOH, 121 °C for 20 min	48	91.0%	(Ashoor and Sukumaran, 2020)
Wild type	10% NaOH, 60 °C for 3 h	48	73.0%	(Chen et al., 2020)
myb103 mutant	Liquid hot water, 200 °C for 30 min	48	79.0%	(Wu et al., 2021)

3.4. Raised dispersion stability of cellulose suspension in the *cesa7* mutant

With respect to the modified cellulose substrate of *cesa7* mutant, this study attempted to explore its potential application for highly valuable bioproducts such as cellulose aerogels. As transforming natural cellulose into stable suspension is the premise for bio-aerogel production and related ultrasonic treatment is an environmentally friendly biomass process (Dilamian and Noroozi, 2021), we first established the optimal ultrasonic treatment conditions at 600 W and 22 kHz, and the parameters of original cellulose concentration and ultrasonic processing volume and time were then optimized according to the final quantity of cellulose suspension (Fig. S2). As a result, the quantity of cellulose suspension was not significantly altered by the change of original cellulose concentrations from 0.4% to 1.2% (m/v), but it was much reduced by the increase of ultrasonic processing volumes from 10 mL to 50 mL (Fig. S2 A, B, D, E). Meanwhile, prolonging ultrasonic time up to 10 min could raise the quantity of cellulose suspension (Fig. S2 C, F), and the optimal conditions were finally evaluated including 0.8% cellulose concentration, 20 mL ultrasonic processing volume and 10 min processing time. As a comparison, the *cesa7* mutant consistently produced more stable cellulose suspensions than those of the NPB (Fig. 5 A, B). In particular, the cellulose substrate of *cesa7* mutant could be completely suspended at 0.28% concentration, whereas the NPB required high concentration at 0.4%. Importantly, while the cellulose emulsion of *cesa7* mutant was dripped or injected into water, it clearly presented teardrop-shaped or linear form, but the NPB showed diffused shapes (Fig. 5 C; Appendix video 1, 2). In addition, the NPB sample started to exhibit the delamination of cellulose suspension from centrifugation at 2000 *g*, but the *cesa7* mutant only appeared at 6000 *g* (Fig. 5 D). Consistently, the *cesa7* mutant had much more cellulose suspensions than those of the NPB after centrifugations at various centrifugal forces (Fig. 5 E). Taken together, the results have thus demonstrated that the *cesa7* mutant could produce much more cellulose suspensions with higher stability, compared to the NPB.

3.5. Improved porosity and specific surface area of cellulose aerogels in the *cesa7* mutant

By performing classic freeze-drying with cellulose suspension, this study generated typical cellulose aerogels in both NPB and *cesa7* samples (Fig. 6). Using cellulose suspensions at a series of concentrations from 0.04% to 0.4%, we examined that the *cesa7* mutant could produce much larger volumes of aerogels than those of the NPB from almost all suspensions samples except 0.4% ones (Fig. 6 A, B). Particularly, the *cesa7* mutant produced the maximum volume (8.2 cm^3) of aerogel from 0.28% cellulose suspension, whereas the aerogel of NPB reached the maximum volume from 0.4% cellulose suspension.

As porosity is an important parameter accounting for cellulose aerogel property (Feng et al., 2021), we detected that both *cesa7* and NPB samples could produce the aerogels with high porosity at more than 99.5%, but the *cesa7* mutant remained relatively higher porosity values than those of the NPB using various concentrations of cellulose suspensions (Fig. 6 C). Furthermore, the *cesa7* mutant was of raised N_2 adsorption-desorption capacities compared to the NPB sample (Fig. 6 D), which confirmed much improved aerogel porosity and specific surface area in the *cesa7* mutant. Based on the compressive strain-stress test, the aerogels from 0.4% cellulose suspensions displayed linear elastic deformation at strains less than 50%. The Young's moduli of NPB and *cesa7* samples were 3.64 kPa and 4.69 kPa, respectively. At 80% strain, the compressive strength of NPB sample was 7.6 kPa, whereas about 8.24 kPa was examined in the *cesa7* sample, indicating a relatively higher flexibility occurred in the *cesa7* sample (Fig. 6 E).

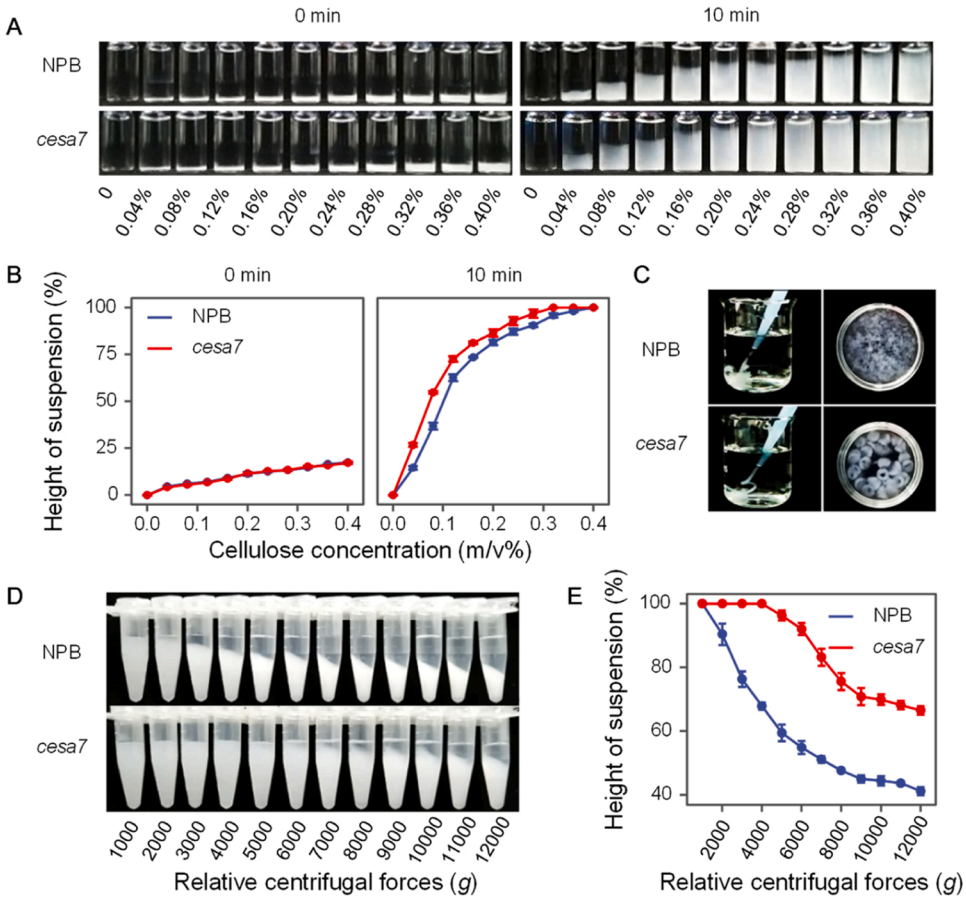

Fig. 5. Dispersion stability of cellulose suspensions from *cesa7* mutant and NPB. (A) Diluted cellulose suspensions at various concentrations from non-ultrasonic (left) or ultrasonic-treatments (right). (B) Quantitative measurement of the quantity of diluted cellulose suspensions in (A). (C) Morphology of cellulose aqueous suspensions after dripping or injecting into water. (D) Cellulose suspensions after centrifugation at relative centrifugal forces from 1000 *g* to 12000 *g*. (E) Quantitative measurement of the relative quantity of cellulose suspensions after centrifugation.

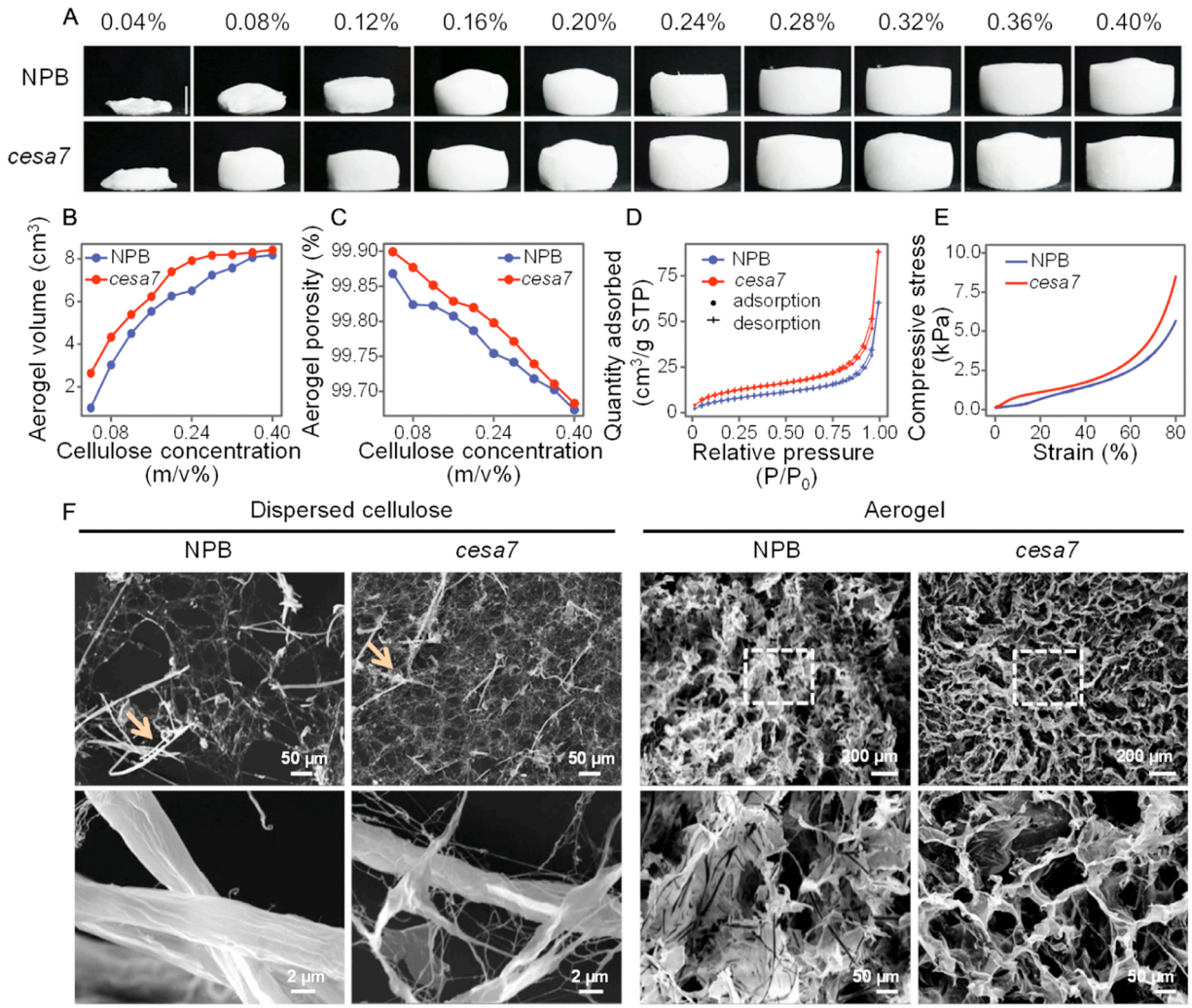

Fig. 6. Characterization of cellulose aerogels from *cesa7* mutant and NPB. (A) Morphology of cellulose aerogels from diluted cellulose suspensions from 0.04% to 0.4% (m/v%). (B) Volumes of cellulose aerogels in (A). (C) Porosity of cellulose aerogels in (A). (D) N_2 adsorption-desorption isotherms of cellulose aerogels from cellulose suspensions at 0.4% (m/v%). (E) Compressive stress-strain curves of cellulose aerogels from cellulose suspensions at 0.4% (m/v%). (F) SEM observation of dispersed cellulose fibers and fabricated aerogels of NPB and *cesa7* mutant.

To understand why the cellulose substrate of *cesa7* mutant could produce high-porosity aerogel, we observed distinct cellulose microfibrils under SEM (Fig. 6 F). Despite the ultrasound-treated cellulose substrates exhibited two types of micro- and nanoscale fibers, the *cesa7* mutant was of relatively higher proportion of nanoscale fibers than those of the NPB. In particular, the NPB sample exhibited relatively large and smooth-surface microfibers, whereas the *cesa7* mutant had small and rough microfibers interlinked with a lot of nanofibrils. Consequently, the *cesa7* aerogel presented a honeycomb-like structure, but the NPB sample showed an irregular sheet-stacked face (Fig. 6 F). The irregular structure of NPB sample might be due to the high crystallinity of cellulose microfibrils against honeycomb-like structure formation during freezing process. Hence, the honeycomb-like structure of *cesa7* mutant should contribute to large surface areas for high oil adsorption capacity as examined below.

3.6. Enhanced oil absorption capacity of cellulose aerogels in the cesa7 mutant

To further test cellulose aerogel property in the *cesa7* mutant, we observed its performance for oil absorption. The cellulose aerogels were modified by methyltrimethoxysilane (MTMS) coating via a chemical vapor deposition process, and the contact angle values of MTMS-modified aerogels (MMA) were more than 120° over the period of 30 s for excellent hydrophobicity (Fig. S3 A). Meanwhile, the silanization of the cellulose substrate was verified by FTIR analysis (Fig. S3 B), indicating adsorption bands at 779 cm^{-1} and 1273 cm^{-1} of MMA for the asymmetric stretching vibration of Si-C and the vibration of Si−CH_3 in the siloxane compound, respectively. Significantly, a positive linear correlation was found between the weights of crosslinked silane and the weights of cellulose at $p < 0.01$ levels in both NPB and *cesa7* samples, but the linear regression slope value of *cesa7* sample was higher than that of the NPB sample (Fig. S3 C, D), suggesting that the cellulose aerogels of *cesa7* sample should be relatively easier for crosslinking, due to a better fibrillation.

While the MMA was applied to absorb pump oil, the *cesa7* mutant sample principally exhibited a higher absorption capacity than that of NPB (Fig. 7 A; Appendix video 3). As the cellulose concentration was raising to 0.28%, the *cesa7* sample was of the highest absorption capacity at 7.1 g, but it was gradually decreasing from higher cellulose concentration (Fig. 7 B), which might be due to much increased cellulose concentration for reduced porosity of aerogels. Despite the absorption capacity of NPB sample was gradually increased from raising cellulose concentrations, its maximum absorption capacity only reached to 5.29 g from 0.4% cellulose concentration (Fig. 7 B). Notably, both NPB and *cesa7* samples exhibited a significantly positive correlation between oil

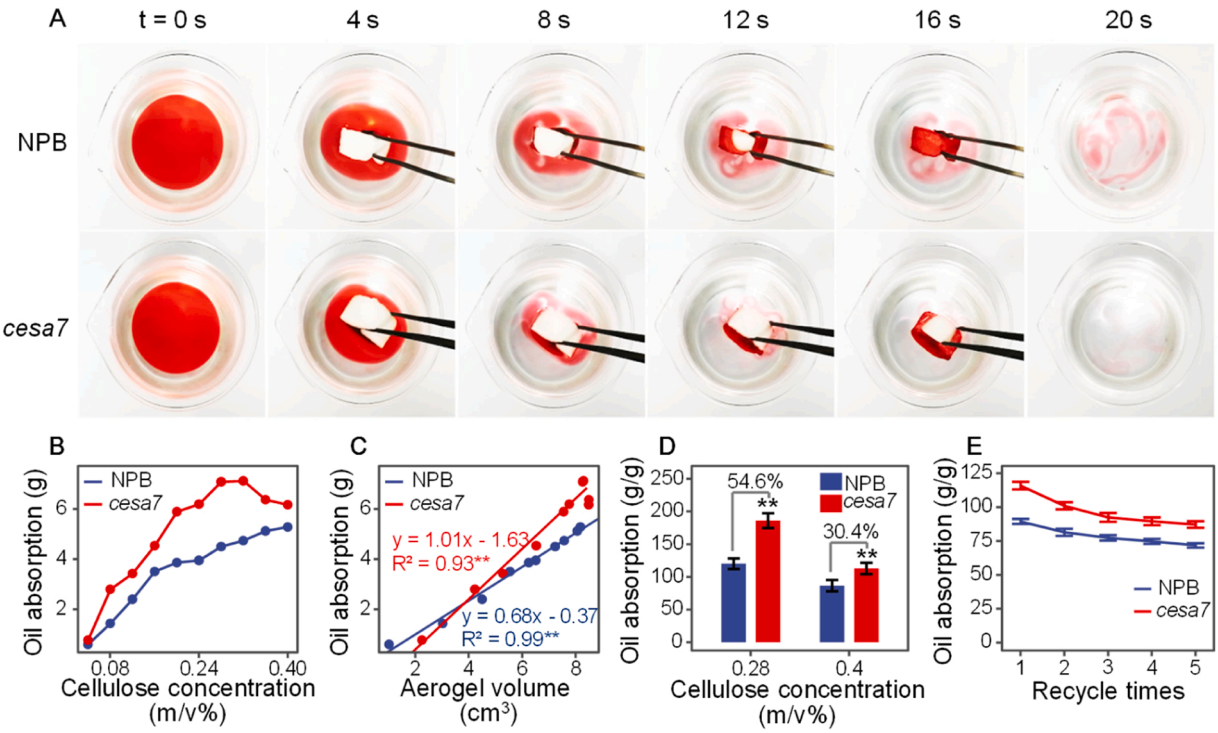

Fig. 7. Oil absorption capacity of MTMS-modified aerogels (MMA) from *cesa7* mutant and NPB. (A) Absorption processes of oil (stained in red) on the surface of the water by MMA. (B) Oil absorption capacity of MMA from diluted cellulose suspensions at various concentrations. (C) Correlation analysis between the aerogel volumes and the oil absorption levels. * * indicated significant correlations at $p < 0.01$. (D) Oil absorption capacity of MMA from diluted cellulose suspensions at 0.28% and 0.4% (n = 6). Increased percentage obtained by subtraction between the data of *cesa7* mutant and NPB divided by the NPB. * * indicated significant difference between two samples by *t*-test at $p < 0.01$. (E) Circulating oil adsorption capacity of MMA from diluted cellulose suspensions at 0.4% (n = 3).

absorption capacity and aerogel volume at $p < 0.01$ level (n = 10) with extremely high R^2 values of 0.99 and 0.93 (Fig. 7 C), which should be accounting for much high oil adsorption with chemical-modified cellulose aerogels. Nevertheless, the *cesa7* sample showed much higher linear regression slope value (1.01) than that of the NPB (0.68), consistent with much raised oil absorption in the *cesa7* sample. Finally, this study calculated the oil absorption per unit weight of aerogel, and the *cesa7* aerogel sample was of oil absorption capacity at 186.2 g /g from 0.28% cellulose concentration, which was higher than that of the NPB sample by 54.6% (Fig. 7 D). Using high concentration of cellulose at 0.4%, the *cesa7* aerogel sample remained much higher oil adsorption capacity than that of the NPB sample by 30.4%. In terms of the speed rate of oil adsorption with aerogels at 0.28% cellulose concentration, the *cesa7* aerogel sample could completely absorb 2 mL oil within 20 s, whereas the NPB aerogel at same size remained part oil unabsorbed (Fig. 7 A; Appendix video 3). The recycling performance of aerogels was further investigated. After 5 cycles, the adsorption capacity of the NPB sample from 0.4% cellulose suspension was decreased from 89.5 g/g to 71.8 g/g, but the *cesa7* sample showed a decreased capacity from 116 g/g to 87.1 g/g (Fig. 7 E), suggesting that the NPB sample should be of slightly better recycling performance. In addition, this work attempted to compare oil adsorption capacity of the *cesa7* aerogel sample with other aerogels generated from different lignocellulose residues in the previous studies, and the *cesa7* aerogel sample researched to the second highest adsorption even though under relatively mild process conditions (Table 2). Therefore, all data have consistently proved that the modified aerogels of *cesa7* sample are of much improved oil adsorption capacity.

Integrating all findings achieved in this study, we proposed a hypothetic model to elucidate how the genetic-modified cellulose substrate is effective for bioethanol and bio-aerogels production in the *cesa7* mutant (Fig. 8). Basically, the site-mutation of OsCESA7 isoform defective at cellulose biosynthesis of plant cell walls could reduce cellulose level and DP in the *cesa7* mutant, leading to either decreased cellulose crystallinity or increased lignocellulose porosity and accessibility. Consequently, those multiple modifications of lignocellulose substrate should cause an integrated enhancement for biomass enzymatic saccharification toward high bioethanol production. Meanwhile, the modified cellulose substrate was more susceptible to fibrillation and enables to efficiently produce aerogels with high porosity and specific surface areas. Due to these improved quality, the chemical-modified aerogels generated from modified cellulose substrates were of much improved oil adsorption capacity. In addition, the increased hemicelluloses and lignin could not only compensate for the cellulose reduction in the *cesa7* mutant to maintain biomass yield, but also relatively enhance plant lodging resistance, probably due to reduced

Table 2
Comparison of oil and organic chemical adsorption of aerogels with the previous works.

Feedstock	Process for cellulose fibrillation	Adsorption capacity of aerogels (g/g)	Reference
***cesa7* straw**	**Sonicated at 22 kHz with 600 W for 10 min**	**180**	**This study**
Rice straw (wild type)	Homogenized at 15,000 rpm for 3 h, and sonicated at 20 kHz with 560 W for 30 min	170	(Dilamian and Noroozi, 2021)
Sugarcane bagasse	Sonicated for 10 min	25	(Thai et al., 2020)
Hardwood pulp	Milled for 0–6000 r	88–228	(Wang et al., 2015)
Oat straw	Homogenized at 20000 rpm for 2 h, and high-shear homogenized for 28 passes	49 – 102	(Zheng et al., 2014)
Cotton linter pulp	Regenerated by NaOH/urea/H_2O	100	(Fu et al., 2020)

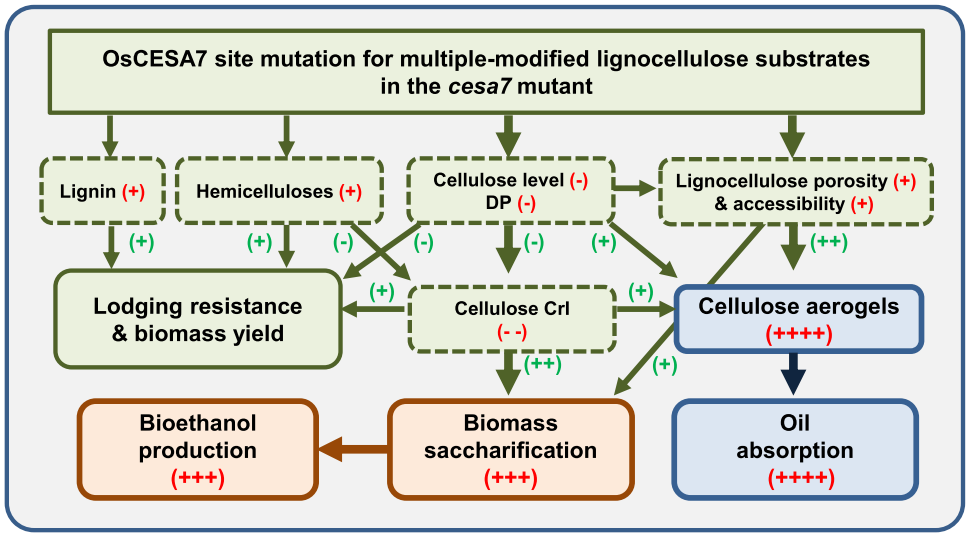

Fig. 8. A hypothetic model to highlight multiple-modified lignocellulose features for relative to its wild type (NPB). Red (+) and (-) as positive and negative lignocellulose factors; Green (+) and (-) as enhanced and decreased processes.

cellulose crystallinity and plant height (Fan et al., 2017). Therefore, this model has highlighted multiple modifications of cellulose substrates for enhancing bioethanol and bioaerogel production in bioenergy crop.

4. Conclusions

By performing specific site-mutation of the OsCESA7 isoform essential for cellulose biosynthesis in plant cell walls, this study selected the desirable rice mutant (*cesa7*) that was of recalcitrance-improved lignocellulose including significantly reduced cellulose features (DP, CrI and nanofibril length) and remarkably raised lignocellulose porosity and accessibility. Due to multiple modifications of cellulose substrate, this study examined near-complete biomass enzymatic saccharification for high bioethanol production under three green-like pretreatments in the *cesa7* mutant, compared to its wild type (NPB). Meanwhile, the modified cellulose substrate of *cesa7* mutant could efficiently produce aerogels with relatively high porosity and specific surface area, and further chemical-modified aerogels were applicable for effective oil adsorption at shorter process time relative to the NPB sample, mainly due to relatively higher proportion of nanoscale fibers and enlarged specific surface areas of the honeycomb-like structure in the *cesa7* sample. Hence, this study has demonstrated multiple-modified cellulose substrate applicable for high bioethanol and bioaerogel production, providing a powerful strategy by integrating genetic modification with mild chemical processes for biofuels and bioproduction under a green-like manner.

CRediT authorship contribution statement

Zhen Hu: Formal analysis, Investigation, Writing – original draft. **Hao Peng:** Formal analysis, Investigation, Writing – review & editing. **Jingyuan Liu:** Validation, Writing – review & editing. **Huiyi Zhang:** Validation, Writing – review & editing. **Sufang Li:** Validation, Writing – review & editing. **Hailang Wang:** Validation, Writing – review & editing. **Zhengyi Lv:** Validation, Writing – review & editing. **Youmei Wang:** Validation, Writing – review & editing. **Dan Sun:** Methodology, Writing – review & editing. **Jingfeng Tang:** Supervision, Writing – review & editing. **Liangcai Peng:** Methodology, Supervision, Writing – review & editing. **Yanting Wang:** Methodology, Supervision, Writing – review & editing, Funding acquisition.

Declaration of Competing Interest

The authors declare that they have no known competing financial interests or personal relationships that could have appeared to influence the work reported in this paper.

Data Availability

Data will be made available on request.

Acknowledgments

This work was in part supported by the National Science Foundation of China (32101701, 32170268) and the National 111 Project of Ministry of Education of China (BP0820035, D17009). We would like to thank Professor Jiankang Zhu and Kabin Xie for their guidance in the rice gene-editing work.

Appendix A. Supporting information

Supplementary data associated with this article can be found in the online version at doi:10.1016/j.indcrop.2023.117044.

References

Alam, A., Zhang, R., Liu, P., Huang, J., Wang, Y., Hu, Z., Madadi, M., Sun, D., Hu, R., Ragauskas, A.J., Tu, Y., Peng, L., 2019. A finalized determinant for complete lignocellulose enzymatic saccharification potential to maximize bioethanol production in bioenergy *Miscanthus*. Biotechnol. Biofuels 12, 99. https://doi.org/10.1186/s13068-019-1437-4.

Alam, A., Wang, Y., Liu, F., Kang, H., Tang, S.W., Cai, Q., Wang, H., Peng, H., Li, Q., Zeng, Y., Tu, Y., Xia, T., Peng, L., 2020. Modeling of optimal green liquor pretreatment for enhanced biomass saccharification and delignification by distinct alteration of wall polymer features and biomass porosity in *Miscanthus*. Renew. Energy 159, 1128–1138. https://doi.org/10.1016/j.renene.2020.06.013.

Ashoor, S., Sukumaran, R.K., 2020. Mild alkaline pretreatment can achieve high hydrolytic and fermentation efficiencies for rice straw conversion to bioethanol. Prep. Biochem. Biotechnol. 50, 814–819. https://doi.org/10.1080/10826068.2020.1744007.

Banoth, C., Sunkar, B., Tondamanati, P.R., Bhukya, B., 2017. Improved physicochemical pretreatment and enzymatic hydrolysis of rice straw for bioethanol production by yeast fermentation. 3 Biotech 7, 334. https://doi.org/10.1007/s13205-017-0980-6.

Bhatia, S.K., Jagtap, S.S., Bedekar, A.A., Bhatia, R.K., Patel, A.K., Pant, D., Banu, J.R., Rao, C.V., Kim, Y.G., Yang, Y.H., 2020. Recent developments in pretreatment technologies on lignocellulosic biomass: Effect of key parameters, technological improvements, and challenges. Bioresour. Technol. 300, 122724 https://doi.org/10.1016/j.biortech.2019.122724.

Bhattacharyya, P., Bhaduri, D., Adak, T., Munda, S., Satapathy, B.S., Dash, P.K., Padhy, S. R., Pattanayak, A., Routray, S., Chakraborti, M., Baig, M.J., Mukherjee, A.K., Nayak, A.K., Pathak, H., 2019. Characterization of rice straw from major cultivars for best alternative industrial uses to cutoff the menace of straw burning. Ind. Crop. Prod. 143, 111919 https://doi.org/10.1016/j.indcrop.2019.111919.

Cantero, D., Jara, R., Navarrete, A., Pelaz, L., Queiroz, J., Rodríguez-Rojo, S., Cocero, M. J., 2019. Pretreatment processes of biomass for biorefineries: current status and prospects. Annu. Rev. Chem. Biomol. Eng. 10, 289–310. https://doi.org/10.1146/annurev-chembioeng-060718-030354.

Chen, C., Deng, X., Kong, W., Qaseem, M.F., Zhao, S., Li, Y., Wu, A.M., 2020. Rice straws with different cell wall components differ on abilities of saccharification. Front. Bioeng. Biotechnol. 8, 624314 https://doi.org/10.3389/fbioe.2020.624314.

Chen, Y., Zhang, L., Yang, Y., Pang, B., Xu, W., Duan, G., Jiang, S., Zhang, K., 2021. Recent progress on nanocellulose aerogels: preparation, modification, composite fabrication, applications. Adv. Mater. 33, 2005569. https://doi.org/10.1002/adma.202005569.

Deng, J., Zhu, X., Chen, P., He, B., Tang, S.W., Zhao, W., Li, X., Zhang, R., Lv, Z., Kang, H., Yu, L., Peng, L., 2020. Mechanism of lignocellulose modification and enzyme disadsorption for complete biomass saccharification to maximize bioethanol yield in rapeseed stalks. Sustain. Energy Fuels 4, 607–618. https://doi.org/10.1039/C9SE00906J.

Dilamian, M., Noroozi, B., 2021. Rice straw agri-waste for water pollutant adsorption: Relevant mesoporous super hydrophobic cellulose aerogel. Carbohydr. Polym. 251, 117016 https://doi.org/10.1016/j.carbpol.2020.117016.

Fan, C., Feng, S., Huang, J., Wang, Y., Wu, L., Li, X., Cai, X., Peng, L., 2017. *AtCesA8*-driven *OsSUS3* expression leads to largely enhanced biomass saccharification and lodging resistance by distinctively altering lignocellulose features in rice. Biotechnol. Biofuels 10, 221. https://doi.org/10.1186/s13068-017-0911-0.

Feng, J., Su, B.L., Xia, H., Zhao, S., Gao, C., Wang, L., Ogbeide, O., Feng, J., Hasan, T., 2021. Printed aerogels: chemistry, processing, and applications. Chem. Soc. Rev. 50, 3842–3888. https://doi.org/10.1039/c9cs00757a.

Fletcher, P.J., van Staden, J.F., 2003. Determination of ethanol in distilled liquors using sequential injection analysis with spectrophotometric detection. Anal. Chim. Acta 499, 123–128. https://doi.org/10.1016/j.aca.2003.07.005.

Fu, B., Yang, Q., Yang, F., 2020. Flexible underwater oleophobic cellulose aerogels for efficient oil/water separation. ACS Omega 5, 8181–8187. https://doi.org/10.1021/acsomega.0c00440.

Fu, Y., Gao, H., Yu, H., Yang, Q., Peng, H., Liu, P., Li, Y., Hu, Z., Zhang, R., Li, J., Qi, Z., Wang, L., Peng, L., Wang, Y., 2022. Specific lignin and cellulose depolymerization of sugarcane bagasse for maximum bioethanol production under optimal chemical fertilizer pretreatment with hemicellulose retention and liquid recycling. Renew. Energy 200, 1371–1381. https://doi.org/10.1016/j.renene.2022.10.049.

Gao, H., Wang, Y., Yang, Q., Peng, H., Li, Y., Zhan, D., Wei, H., Lu, H., Bakr, M., Ei-Sheekh, M.M., Qi, Z., Peng, L., Lin, X., 2021. Combined steam explosion and optimized green-liquor pretreatments are effective for complete saccharification to maximize bioethanol production by reducing lignocellulose recalcitrance in one-year-old bamboo. Renew. Energy 175, 1069–1079. https://doi.org/10.1016/j.renene.2021.05.016.

Gu, F., Wang, W., Jing, L., Jin, Y., 2013. Effects of green liquor pretreatment on the chemical composition and enzymatic digestibility of rice straw. Bioresour. Technol. 149, 375–382. https://doi.org/10.1016/j.biortech.2013.09.064.

Himmel, M.E., Ding, S.Y., Johnson, D.K., Adney, W.S., Nimlos, M.R., Brady, J.W., Foust, T.D., 2007. Biomass recalcitrance: engineering plants and enzymes for biofuels production. Science 315, 804–807. https://doi.org/10.1126/science.1137016.

Hu, Z., Zhang, G., Muhammad, A., Samad, R.A., Wang, Y., Walton, J.D., He, Y., Peng, L., Wang, L., 2018. Genetic loci simultaneously controlling lignin monomers and biomass digestibility of rice straw. Sci. Rep. 8, 3636. https://doi.org/10.1038/s41598-018-21741-y.

Hu, Z., Wang, Y., Liu, J., Li, Y., Wang, Y., Huang, J., Ai, Y., Chen, P., He, Y., Aftab, M.N., Wang, L., Peng, L., 2021. Integrated NIRS and QTL assays reveal minor mannose and galactose as contrast lignocellulose factors for biomass enzymatic saccharification in rice. Biotechnol. Biofuels 14, 144. https://doi.org/10.1186/s13068-021-01987-x.

Hu, Z., Li, Q., Chen, Y., Li, T., Wang, Y., Zhang, R., Peng, H., Wang, H., Wang, Y., Tang, J., Aftab, M.N., Peng, L., 2023. Intermittent ultrasound retains cellulases unlock for enhanced cellulosic ethanol with high-porosity biochar for dye adsorption using desirable rice mutant straw. Bioresour. Technol. 369, 128437 https://doi.org/10.1016/j.biortech.2022.128437.

Huang, J., Li, Y., Wang, Y., Chen, Y., Liu, M., Wang, Y., Zhang, R., Zhou, S., Li, J., Tu, Y., Hao, B., Peng, L., Xia, T., 2017. A precise and consistent assay for major wall polymer features that distinctively determine biomass saccharification in transgenic rice by near-infrared spectroscopy. Biotechnol. Biofuels 10, 294. https://doi.org/10.1186/s13068-017-0983-x.

Huang, J., Xia, T., Li, G., Li, X., Li, Y., Wang, Y., Chen, Y., Xie, G., Bai, F.W., Peng, L., Wang, L., 2019. Overproduction of native endo-β-1, 4-glucanases leads to largely enhanced biomass saccharification and bioethanol production by specific modification of cellulose features in transgenic rice. Biotechnol. Biofuels 12, 11. https://doi.org/10.1186/s13068-018-1351-1.

Jiang, F., Hsieh, Y.L., 2017. Cellulose nanofibril aerogels: synergistic improvement of hydrophobicity, strength, and thermal stability via cross-linking with diisocyanate. ACS Appl. Mater. Interfaces 9, 2825–2834. https://doi.org/10.1021/acsami.6b13577.

Jiang, F., Han, S., Hsieh, Y.L., 2013. Controlled defibrillation of rice straw cellulose and self-assembly of cellulose nanofibrils into highly crystalline fibrous materials. RSC Adv. 3, 12366–12375. https://doi.org/10.1039/c3ra41646a.

Jin, W., Chen, L., Hu, M., Sun, D., Li, A., Li, Y., Hu, Z., Zhou, S., Tu, Y., Xia, T., Wang, Y., Xie, G., Li, Y., Bai, B., Peng, L., 2016. Tween-80 is effective for enhancing steam-exploded biomass enzymatic saccharification and ethanol production by specifically lessening cellulase absorption with lignin in common reed. Appl. Energy 175, 82–90. https://doi.org/10.1016/j.apenergy.2016.04.104.

Li, F., Xie, G., Huang, J., Zhang, R., Li, Y., Zhang, M., Wang, Y., Li, A., Li, X., Xia, T., Qu, C., Hu, F., Ragauskas, A.J., Peng, L., 2017. OsCESA9 conserved-site mutation leads to largely enhanced plant lodging resistance and biomass enzymatic saccharification by reducing cellulose DP and crystallinity in rice. Plant Biotechnol. J. 15, 1093–1104. https://doi.org/10.1111/pbi.12700.

Li, Y., Liu, P., Huang, J., Zhang, R., Hu, Z., Feng, S., Wang, Y., Wang, L., Tao, X., Peng, L., 2018. Mild chemical pretreatments are sufficient for bioethanol production in transgenic rice straws overproducing glucosidase. Green Chem. 20, 2047–2056. https://doi.org/10.1039/c8gc00694f.

Liu, H., Ding, Y., Zhou, Y., Jin, W., Xie, K., Chen, L.L., 2017. CRISPR-P 2.0: an improved CRISPR-Cas9 tool for genome editing in plants. Mol. Plant 10, 530–532. https://doi.org/10.1016/j.molp.2017.01.003.

Liu, W., Deng, Y., Hussain, S., Zou, J., Yuan, J., Luo, L., Yang, C., Yuan, X., Yang, W., 2016. Relationship between cellulose accumulation and lodging resistance in the stem of relay intercropped soybean [*Glycine max* (L.) Merr.]. Field Crop. Res. 196, 261–267. https://doi.org/10.1016/j.fcr.2016.07.008.

Ma, Y., Sawhney, V.K., Steeves, T.A., 1993. Staining of paraffin-embedded plant material in safranin and fast green without prior removal of the paraffin. Can. J. Bot. 71, 996–999. https://doi.org/10.1139/b93-114.

Peng, H., Zhao, W., Liu, J., Liu, P., Yu, H., Deng, J., Yang, Q., Zhang, R., Hu, Z., Liu, S., Sun, D., Peng, L., Wang, Y., 2022. Distinct cellulose nanofibrils generated for improved Pickering emulsions and lignocellulose-degradation enzyme secretion coupled with high bioethanol production in natural rice mutants. Green Chem. 24, 2975–2987. https://doi.org/10.1039/d1gc04447h.

Sun, D., Yang, Q., Wang, Y., Gao, H., He, M., Lin, X., Lu, J., Wang, Y., Kang, H., Alam, A., Tu, Y., Xia, T., Peng, L., 2020. Distinct mechanisms of enzymatic saccharification and bioethanol conversion enhancement by three surfactants under steam explosion and mild chemical pretreatments in bioenergy *Miscanthus*. Ind. Crop. Prod. 153, 112559 https://doi.org/10.1016/j.indcrop.2020.112559.

Tanaka, K., Murata, K., Yamazaki, M., Onosato, K., Miyao, A., Hirochika, H., 2003. Three distinct rice cellulose synthase catalytic subunit genes required for cellulose synthesis in the secondary wall. Plant Physiol. 133, 73–83. https://doi.org/10.1104/pp.103.022442.

Teo, H.L., Wahab, R.A., 2020. Towards an eco-friendly deconstruction of agro-industrial biomass and preparation of renewable cellulose nanomaterials: a review. Int. J. Biol. Macromol. 161, 1414–1430. https://doi.org/10.1016/j.ijbiomac.2020.08.076.

Thai, Q.B., Nguyen, S.T., Ho, D.K., Tran, T.D., Huynh, D.M., Do, N.H.N., Luu, T.P., Le, P. K., Le, D.K., Phan-Thien, N., Duong, H.M., 2020. Cellulose-based aerogels from sugarcane bagasse for oil spill-cleaning and heat insulation applications. Carbohydr. Polym. 228, 115365 https://doi.org/10.1016/j.carbpol.2019.115365.

Wang, S., Peng, X., Zhong, L., Tan, J., Jing, S., Cao, X., Chen, W., Liu, C., Sun, R., 2015. An ultralight, elastic, cost-effective, and highly recyclable superabsorbent from microfibrillated cellulose fibers for oil spillage cleanup. J. Mater. Chem. A 3, 8772–8781. https://doi.org/10.1039/c4ta07057g.

Wang, Y., Liu, P., Zhang, G., Yang, Q., Lu, J., Xia, T., Peng, L., Wang, Y., 2021. Cascading of engineered bioenergy plants and fungi sustainable for low-cost bioethanol and high-value biomaterials under green-like biomass processing. Renew. Sustain. Energy Rev. 137, 110586 https://doi.org/10.1016/j.rser.2020.110586.

Wu, L., Feng, S., Deng, J., Yu, B., Wang, Y., He, B., Peng, H., Li, Q., Hu, R., Peng, L., 2019. Altered carbon assimilation and cellulose accessibility to maximize bioethanol yield under low-cost biomass processing in corn brittle stalk. Green Chem. 21, 4388–4399. https://doi.org/10.1039/c9gc01237k.

Wu, L., Zhang, M., Zhang, R., Yu, H., Wang, H., Li, J., Wang, Y., Hu, Z., Luo, Z., Li, L., Wang, L., Peng, L., Xia, T., 2021. Down-regulation of *OsMYB103L* distinctively alters beta-1, 4-glucan polymerization and cellulose microfibers assembly for enhanced biomass enzymatic saccharification in rice. Biotechnol. Biofuels 14, 245. https://doi.org/10.1186/s13068-021-02093-8.

Xie, K., Zhang, J., Yang, Y., 2014. Genome-wide prediction of highly specific guide RNA spacers for CRISPR-Cas9-mediated genome editing in model plants and major crops. Mol. Plant 7, 923–926. https://doi.org/10.1093/mp/ssu009.

Xie, K., Minkenberg, B., Yang, Y., 2015. Boosting CRISPR/Cas9 multiplex editing capability with the endogenous tRNA-processing system. Proc. Natl. Acad. Sci. USA 112, 3570–3575. https://doi.org/10.1073/pnas.1420294112.

Xu, N., Zhang, W., Ren, S., Liu, F., Zhao, C., Liao, H., Xu, Z., Huang, J., Li, Q., Tu, Y., Yu, B., Wang, Y., Jiang, J., Qin, J., Peng, L., 2012. Hemicelluloses negatively affect lignocellulose crystallinity for high biomass digestibility under NaOH and H_2SO_4 pretreatments in *Miscanthus*. Biotechnol. Biofuels 5, 58. https://doi.org/10.1186/1754-6834-5-58.

Xu, S., Wang, R., Gasser, T., Ciais, P., Peñuelas, J., Balkanski, Y., Boucher, O., Janssens, I. A., Sardans, J., Clark, J.H., Cao, J., Xing, X., Chen, J., Wang, L., Tang, X., Zhang, R., 2022. Delayed use of bioenergy crops might threaten climate and food security. Nature 609, 299–306. https://doi.org/10.1038/s41586-022-05055-8.

Yao, R.S., Hu, H.J., Deng, S.S., Wang, H., Zhu, H.X., 2011. Structure and saccharification of rice straw pretreated with sulfur trioxide micro-thermal explosion collaborative dilutes alkali. Bioresour. Technol. 102, 6340–6343. https://doi.org/10.1016/j.biortech.2011.02.073.

Zhang, G., Wang, L., Li, X., Bai, S., Xue, Y., Li, Z., Tang, S., Wang, Y., Wang, Y., Hu, Z., Li, P., Peng, L., 2020. Distinctively altered lignin biosynthesis by site-modification of *OsCAD2* for enhanced biomass saccharification in rice. GCB Bioenergy 13, 305–319. https://doi.org/10.1111/gcbb.12772.

Zhang, M., Wei, F., Guo, K., Hu, Z., Li, Y., Xie, G., Wang, Y., Cai, X., Peng, L., Wang, L., 2016. A novel *FC116/BC10* mutation distinctively causes alteration in the expression of the genes for cell wall polymer synthesis in rice. Front. Plant Sci.. 7, 1366. https://doi.org/10.3389/fpls.2016.01366.

Zhang, R., Hu, Zhen, Peng, H., Liu, P., Wang, Y., Li, J., Lu, J., Wang, Y., Xia, T., Peng, L., 2023. High density cellulose nanofibril assembly leads to upgraded enzymatic and chemical catalysis of fermentable sugars, cellulose nanocrystals and cellulase production by precisely engineering cellulose synthase complexes. Green Chem. 25, 1096. https://doi.org/10.1039/d2gc03744k.

Zhang, X., Liu, M., Wang, H., Yan, N., Cai, Z., Yu, Y., 2019. Ultralight, hydrophobic, anisotropic bamboo-derived cellulose nanofibrils aerogels with excellent shape recovery via freeze-casting. Carbohydr. Polym. 208, 232–240. https://doi.org/10.1016/j.carbpol.2018.12.073.

Zheng, Z., Sèbe, G., Rentsch, D., Zimmermann, T., Tingaut, P., 2014. Ultralightweight and flexible silylated nanocellulose sponges for the selective removal of oil from water. Chem. Mater. 26, 2659–2668. https://doi.org/10.1021/cm5004164.